3-9-2007

Unraveling the Catalytic Mechanism of Nitrile Hydratases

Sanghamitra Mitra
Utah State University

Richard C. Holz
Marquette University, richard.holz@marquette.edu

Published version. *Journal of Biological Chemistry*, Vol. 282, No. 10 (March 9, 2007): 7397-7404. DOI.
Richard Holz was affiliated with the Loyola University of Chicago at the time of publication.

THE JOURNAL OF BIOLOGICAL CHEMISTRY VOL. 282, NO. 10, pp. 7397–7404, March 9, 2007

Unraveling the Catalytic Mechanism of Nitrile Hydratases*

Received for publication, May 1, 2006, and in revised form, December 5, 2006 Published, JBC Papers in Press, December 6, 2006, DOI 10.1074/jbc.M604117200

Sanghamitra Mitra[‡] **and Richard C. Holz**[‡§1]

From the [‡]*Department of Chemistry and Biochemistry, Utah State University, Logan, Utah 84322-0300 and the* [§]*Department of Chemistry, Loyola University, Chicago, Illinois 60626*

To elucidate a detailed catalytic mechanism for nitrile hydratases (NHases), the pH and temperature dependence of the kinetic constants k_{cat} and K_m for the cobalt-type NHase from *Pseudonocardia thermophila* JCM 3095 (*Pt*NHase) were examined. *Pt*NHase was found to exhibit a bell-shaped curve for plots of relative activity *versus* pH at pH 3.2–11 and was found to display maximal activity between pH 7.2 and 7.8. Fits of these data provided pK_{ES1} and pK_{ES2} values of 5.9 ± 0.1 and 9.2 ± 0.1 ($k_{cat}' = 130 \pm 1\ s^{-1}$), respectively, and p$K_{E1}$ and pK_{E2} values of 5.8 ± 0.1 and 9.1 ± 0.1 ($k_{cat}'/K_m' = (6.5 \pm 0.1) \times 10^3\ s^{-1}\ mM^{-1}$), respectively. Proton inventory studies indicated that two protons are transferred in the rate-limiting step of the reaction at pH 7.6. Because *Pt*NHase is stable at 60 °C, an Arrhenius plot was constructed by plotting ln(k_{cat}) *versus* $1/T$, providing E_a = 23.0 ± 1.2 kJ/mol. The thermal stability of *Pt*NHase also allowed ΔH^0 ionization values to be determined, thus helping to identify the ionizing groups exhibiting the pK_{ES1} and pK_{ES2} values. Based on ΔH^0_{ion} data, pK_{ES1} is assigned to βTyr^{68}, whereas pK_{ES2} is assigned to βArg^{52}, βArg^{157}, or αSer^{112} (NHases are $\alpha_2\beta_2$-heterotetramers). A combination of these data with those previously reported for NHases and synthetic model complexes, along with sequence comparisons of both iron- and cobalt-type NHases, allowed a novel catalytic mechanism for NHases to be proposed.

Nitrile hydratase (NHase[2]; EC 4.2.1.84), one of the enzymes in the nitrile degradation pathway, catalyzes the hydrolysis of nitriles to their corresponding higher value amides in a chemo-, regio-, and/or enatioselective manner at ambient pressures and temperatures at physiological pH (Scheme 1) (1–6). NHases have attracted substantial interest as biocatalysts for industrial applications such as the large-scale production of acrylamide (3, 7–9) and nicotinamide (10). Acrylamide production utilizing the bacterium *Rhodococcus rhodochrous* J1 has increased to >30,000 tons/year (3), whereas >3500 tons of nicotinamide are produced per year (11). Yields of >99% are achieved, and the formation of by-products such as acrylic acid, which plagues traditional methodology, is completely avoided. However, one of the most attractive features of nitrile-metabolizing enzymes is their ability to selectively hydrolyze one cyano group of a dinitrile to its corresponding amine, something that is virtually impossible using conventional chemical methods (12–14). Therefore, the potential use of nitrile-hydrolyzing enzymes for the production of several fine chemicals is increasingly recognized.

NHases are metalloenzymes that contain either a non-heme Fe(III) ion (iron-type) or a non-corrin Co(III) ion (cobalt-type) in their active site and are typically $\alpha_2\beta_2$-heterotetramers (5, 6, 15, 16). In all known NHases, each α-subunit has a highly homologous amino acid sequence (C*X*YCSC*X*) that forms the metal-binding site. Cobalt-type NHases contain threonine and tyrosine in the -C(T/S)YCSC(Y/T)- sequence of the active center, whereas iron-type NHases contain serine and threonine (6). Recently, both iron- and cobalt-type NHases have been crystallographically characterized (17–22). In all structures published to date, the trivalent metal ion is six-coordinate, with the remaining ligands made up of three cysteines and two amide nitrogens (Fig. 1). Interestingly, two of the active-site cysteine residues are post-translationally modified to cysteinesulfinic acid (–SO_2H) and cysteinesulfenic acid (–SOH), yielding an unusual metal coordination geometry termed a "claw setting," and it has been shown that, unless this Cys oxidation process occurs, NHase is inactive (23, 24). In iron-type NHases, nitric oxide (NO) binds in place of a metal-coordinated water/hydroxide molecule, which can be photoactivated, whereas cobalt-type NHases do not bind NO (5). Based on theoretical calculations, the carbon–nitrogen bond in the coordinated amide of both iron- and cobalt-type NHases has significant double bond character, suggesting that it is best represented as an imidometal bond (25).

The structural characterization of both iron- and cobalt-type NHases has provided some insight into how the molecular structure controls the enzyme function. Based on these data and several elegant studies on active-site NHase model complexes (for reviews, see Refs. 5 and 16), four simple reaction mechanisms have been proposed (5, 26). In each reaction, imidate is produced as a reaction intermediate, which then isomerizes to the corresponding amide. Even though a significant amount of structural and synthetic modeling data have been reported for NHases, details of the enzymatic reaction, including which proposed mechanism is operative as well as the nature of the transition state, the identities of groups involved in proton transfers, and the role of the metal ion, remain uncertain. To gain insight into the catalytically important active-site residues and the number of protons that are transferred in the transition state, we have examined the pH and temperature

* This work was supported by National Science Foundation Grant CHE 0652981 (to R. C. H.). The costs of publication of this article were defrayed in part by the payment of page charges. This article must therefore be hereby marked "*advertisement*" in accordance with 18 U.S.C. Section 1734 solely to indicate this fact.

[1] To whom correspondence should be addressed: Dept. of Chemistry, Loyola University, 1068 West Sheridan Rd., Chicago, IL 60626. Tel.: 773-508-3092; Fax: 773-508-3086; E-mail: rholz1@luc.edu.

[2] The abbreviations used are: NHase, nitrile hydratase; *Pt*NHase, *P. thermophila* JCM 3095 cobalt-type nitrile hydratase; MOPS, 4-morpholinepropanesulfonic acid; MES, 4-morpholineethanesulfonic acid.

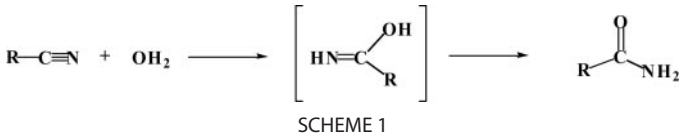

SCHEME 1

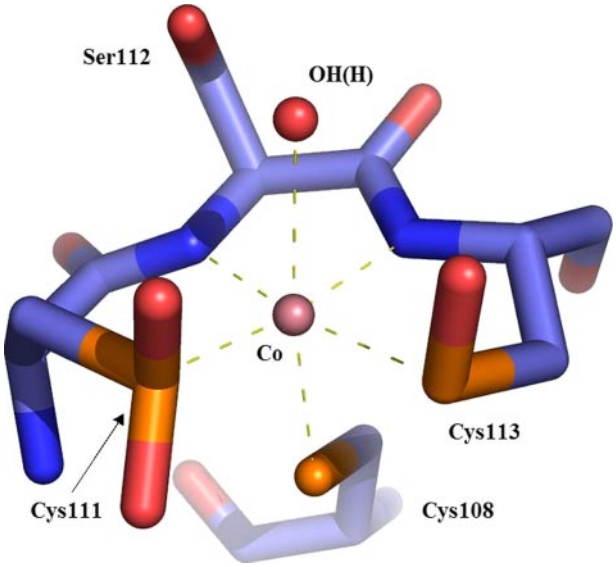

FIGURE 1. **Active site of NHase from *P. thermophila* (Protein Data Bank code 1IRE).** The trivalent metal ion is six-coordinate, with three cysteine sulfurs, two amide nitrogens, and one water molecule. Cys^{111} is post-translationally modified to cysteinesulfinic acid, and Cys^{113} is modified to cysteinesulfenic acid (20, 21).

dependence of the kinetic parameters and solvent isotope effect of the cobalt-type NHase from *Pseudonocardia thermophila* JCM 3095 (*Pt*NHase). Based on these data, a novel catalytic mechanism is proposed.

MATERIALS AND METHODS

Protein Expression, Purification, and Kinetic Assay—All chemicals used in this study were purchased from commercial sources and were of the highest quality available. The plasmid encoding the α- and β-subunits of *Pt*NHase was obtained from the International Patent Organism Depositary (unit.aist.go.jp/ipod/index_e.html) in Japan. The enzyme was purified by a significantly simplified and shortened procedure based on a previously published purification method (19, 20). Briefly, *Escherichia coli* BL21 Star™(DE3) cells containing the pUC18-NHase plasmid (20), which includes the genes for the α- and β-subunits of NHase and an NHase activator protein, were grown at 37 °C in 5 liters of Luria-Bertani broth containing ampicillin (100 mg/liter). When the absorbance reached ~0.8 at 600 nm, the cells were induced by the addition of 0.1 mM isopropyl β-D-thiogalactopyranoside and 0.25 mM Co(II) chloride. The cells were then cultured for an additional 16 h, followed by harvesting by centrifugation. All subsequent manipulations were performed at 4 °C. The cell paste was resuspended in 10 ml of 50 mM Tris-HCl (pH 7.6), sonicated, and clarified by centrifugation. The cell-free extract was fractionated with 40–70% ammonium sulfate and equilibrated with 50 mM phosphate buffer (pH 7.6) containing 1 M $(NH_4)_2SO_4$ prior to hydrophobic interaction gradient chromatographic purification using phenyl-Sepharose (1 M $(NH_4)_2SO_4$ and 0% isopropyl alcohol → 0 M $(NH_4)_2SO_4$ and 0% isopropyl alcohol → 0 M $(NH_4)_2SO_4$ and 40% isopropyl alcohol). Active fractions (~15% isopropyl alcohol) were concentrated by ultrafiltration and further purified to >95% (SDS-PAGE) by size exclusion chromatography using Sephacryl S-300.

*Pt*NHase was assayed for catalytic activity using benzonitrile as the substrate (20). In this assay, the hydration of benzonitrile was measured spectrophotometrically by monitoring the formation of benzamide at 242 nm (ϵ = 5.5 mM^{-1} cm^{-1}). All assays were performed on a Shimadzu UV-3101PC spectrophotometer equipped with a constant-temperature cell holder and an ISOTEMP 2013D water bath (Fisher). Enzyme concentrations were determined using the Bradford assay with bovine serum albumin as the standard. All assays were performed at 25 ± 0.1 °C in 50 mM potassium phosphate buffer (pH 7.6).

pH Profiles—The enzymatic activities of *Pt*NHase at pH 3.2–11.0 were measured using benzonitrile as the substrate. The concentration of each buffer used was 50 mM, and the following buffers were used: borate (pH 8.50–10.50), Tris-HCl (pH 7.00–8.50), phosphate (pH 7.00–7.75), MOPS (pH 6.50–7.00), MES (pH 5.50–6.50), and acetate (pH 3.23–5.50). The kinetic parameters k_{cat}, K_m, and k_{cat}/K_m were determined using 8–12 different substrate concentrations ranging from 0.2 to 10.0 times the observed K_m value at each pH studied. Kinetic parameters and fits to the kinetic curves were obtained using IGOR Pro (WaveMetrics, Lake Oswego, OR).

Solvent Isotope Effect—All buffers were prepared from a freshly opened bottle of 99.9% ^2H_2O (Aldrich). The buffers used in the preparation of all deuterated buffers were in the anhydrous form. The pH of each buffer used was adjusted by the addition of NaOD or DCl (both 99%+ deuterium content; Acros Organics, Geel, Belgium) and corrected for deuteration by adding 0.4 to the reading of the pH electrode (27).

RESULTS

pH Dependence of the Kinetic Parameters—To examine the reaction mechanism of *Pt*NHase, the kinetic parameters k_{cat}, K_m, and k_{cat}/K_m were recorded as a function of pH. *Pt*NHase catalyzed the hydration of benzonitrile at pH 7.6 and 25 °C with $k_{cat} = 123 \pm 1\ s^{-1}$ and $K_m = 20.0 \pm 0.1\ \mu M$ in the absence of *n*-butyric acid. These values are indistinguishable from those reported previously ($k_{cat} = 120\ s^{-1}$ and K_m = 19 μM) (20). *Pt*NHase was found to exhibit a bell-shaped curve for plots of relative activity *versus* pH at pH 3.2–11 and was found to display maximal activity between pH 7.2 and 7.8. Plots of $\log(k_{cat})$ and $\log(k_{cat}/K_m)$ *versus* pH were prepared for *Pt*NHase and fit to Equations 1 and 2, respectively (Fig. 2) (28, 29),

$$\log(k_{cat}) = \log(k_{cat}'/(1 + [H]/K_{ES1} + K_{ES2}/[H])) \quad \text{(Eq. 1)}$$

$$\log(k_{cat}/K_m) = \log(k_{cat}'/K_m'/(1 + [H]/K_{E1} + K_{E2}/[H])) \quad \text{(Eq. 2)}$$

where k_{cat}' is the theoretical maximal velocity; k_{cat}'/K_m' is the theoretical maximal catalytic efficiency; K_{ES1} is the ionization constant of the *ES* complex that affects the acidic side of the pH curve; K_{ES2} reflects the basic side; and K_{E1} and K_{E2} are the ion-

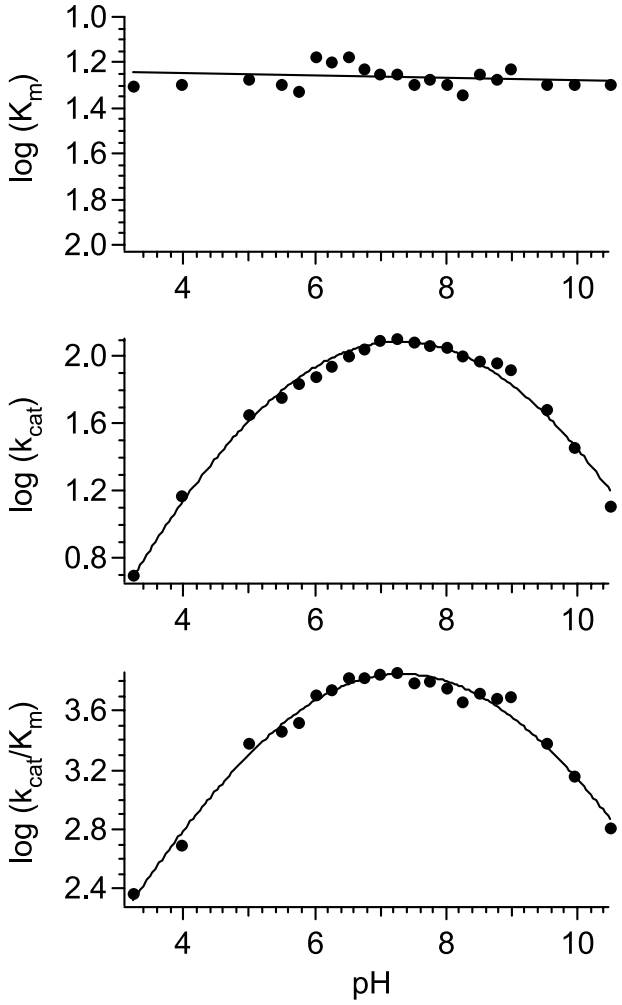

FIGURE 2. **pH dependence of the kinetic parameters for the hydration of benzonitrile by *Pt*NHase between pH 3.2 and 11.** The K_m does not vary with pH. The pH dependence of k_{cat} fit to Equation 1, and the pH dependence of k_{cat}/K_m fit to Equation 2. The kinetic constants obtained from the fits are listed in Table 1. *Error bars* are smaller than the symbols used.

ization constants for an acidic and basic group, respectively, on the free enzyme or free substrate.

$$\begin{array}{ccc} E^{1-} & & E^{1-}\cdot S \\ \uparrow\downarrow K_{E1} & & \uparrow\downarrow K_{ES2} \\ EH + S & \rightleftharpoons & EH\cdot S \rightleftharpoons EP \\ \uparrow\downarrow K_{E2} & & \uparrow\downarrow K_{ES1} \\ EH_2^{1+} & & EH_2^{1+}\cdot S \end{array}$$

SCHEME 2

Inspection of a plot of log(K_m) *versus* pH (Fig. 2) indicated that the K_m does not vary with pH. Therefore, plots of log(k_{cat}) *versus* pH and plots of log(k_{cat}/K_m) *versus* pH provided similar pK_a values (Table 1).

Examination of a plot of log(k_{cat}) *versus* pH revealed a bell-shaped curve that could be fit to Equation 1 (Fig. 2). The slopes of the asymptotes, calculated as described previously (30), for the acidic and basic limbs of log(k_{cat}) *versus* pH for *Pt*NHase are 1, indicating that one group is ionized on each limb. A good fit to Equation 1 was obtained, which yielded a pK_{ES1} value of 5.9 ± 0.1 and a pK_{ES2} value of 9.2 ± 0.1 ($k_{cat}' = 130 \pm 1\ s^{-1}$). Similar

TABLE 1
Ionization constants for benzonitrile hydration by *Pt*NHase

k_{cat} *vs.* pH	
pK_{ES1}	5.9 ± 0.1
pK_{ES2}	9.2 ± 0.1
k_{cat}' (s^{-1})	130 ± 1
k_{cat}/K_m *vs.* pH	
pK_{E1}	5.8 ± 0.1
pK_{E2}	9.1 ± 0.1
k_{cat}'/K_m' ($s^{-1}\ mM^{-1}$)	(6.5 ± 0.1) × 10^3

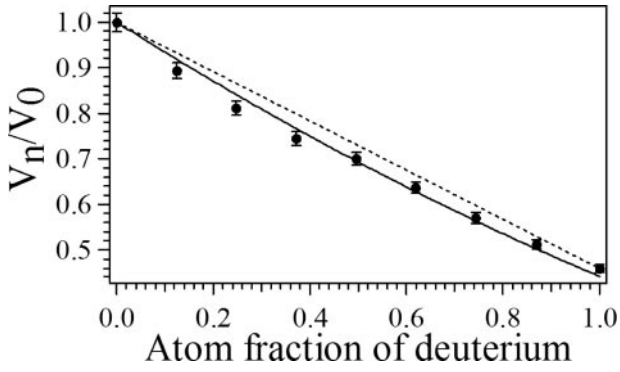

FIGURE 3. **Plot of V_n/V_0 *versus* the atom fraction of deuterium for *Pt*NHase at pH 7.6.** V_n/V_0 is defined as (velocity at *n* atom fraction of deuterium)/(velocity in water). The *dashed line* represents a linear relationship; the *solid line* is a direct fit to Equation 4 with fractionation factors $\phi_{T1} = 0.66$ and $\phi_{T2} = 0.68$.

to plots of log(k_{cat}) *versus* pH, fits of log(k_{cat}/K_m) *versus* pH to Equation 2 provided a pK_{E1} value of 5.8 ± 0.1 and a pK_{E2} value of 9.1 ± 0.1 ($k_{cat}'/K_m' = (6.5 \pm 0.1) \times 10^3\ s^{-1}\ mM^{-1}$) (Fig. 2).

Solvent Isotope Effect—Solvent isotope effect experiments were carried out on *Pt*NHase using benzonitrile as the substrate at pH 7.6 ($p^2H = p^1H$ meter reading + 0.4) (27) by substituting hydrogen (^1H) with deuterium (^2H). k_{cat} values for benzonitrile were measured at several different ratios of D_2O and H_2O, and the results were plotted as the atom fraction of deuterium *versus* V_n/V_0, where V_n is the observed velocity at *n* fraction of deuterium, and V_0 is the observed velocity in water (Fig. 3). Proton inventories were obtained by fitting the experimental data to equations derived from the Gross-Butler equation (Equation 3),

$$V_n/V_0 = \frac{\prod_i^{\nu_T}(1 - n + n\phi_i^T)}{\prod_j^{\nu_R}(1 - n + n\phi_i^R)} \qquad \text{(Eq. 3)}$$

where *n* is the atom fraction of deuterium, ν_T is the number of protons transferred in the transition state, ν_R is the number of protons transferred in the reactant state, and ϕ is the fractionation factor defined as in Equation 4,

$$\phi = (X_i^D/X_i^H)/(n/(1 - n)) \qquad \text{(Eq. 4)}$$

where X_i^D and X_i^H are the mole fractions of deuterons and protons in the *i*th transition or reactant state (31, 32). At pH 7.6, the data deviate from linearity, and the best fit was obtained for a polynomial, suggesting that at least two protons are transferred in the transition state at this pH (Fig. 3). Because the largest deviation for theoretical proton inventory curves occurs at an

TABLE 2

Comparison of experimental and calculated midpoint solvent isotope effects

The experiment was carried out using benzonitrile as the substrate at pH 7.6. Experimental and theoretical midpoint isotope effects were calculated for 0.49 atom fraction of deuterium.

	V_0/V_1	Midpoint solvent isotope effect (V_m/V_1)	Calculated midpoint solvent isotope effect		
			One proton	Two protons	Generalized solvation changes
*Pt*NHase	2.07	1.45	1.53	1.45	1.43

TABLE 3

Thermodynamic parameters for benzonitrile hydration by *Pt*NHase at 25 °C

$E + S \rightarrow ES$	
ΔG^0 (kJ/mol)	−7.3 ± 0.4
ΔH^0 (kJ/mol)	−10.2 ± 0.5
ΔS^0 (J/mol)	−9.7 ± 0.7
$ES \rightarrow (ES\cdot\cdot EP)^{\ddagger}$	
$\Delta G^{\ddagger}$ (kJ/mol)	61.1 ± 1.0
$\Delta H^{\ddagger}$ (kJ/mol)	18.0 ± 0.9
$\Delta S^{\ddagger}$ (J/mol)	−146.0 ± 0.7
E_a (kJ/mol)	23.0 ± 1.2

atom fraction of 0.5 (33, 34), calculation of a midpoint partial solvent isotope effect often helps in determining the number of protons involved in the catalytic reaction. Equations 5–7, derived by Elrod *et al.* (33), allowed the calculation of midpoint partial solvent isotope effects when the experimental data were obtained at different atom fractions,

$$\text{One proton: } V_m/V_1 = (1 - n_m)(V_0/V_1) + n_m \quad \text{(Eq. 5)}$$

$$\text{Two protons: } (V_m/V_1) = ((1 - n_m)(V_0/V_1)^{1/2} + n_m)^2 \quad \text{(Eq. 6)}$$

$$\text{General solvation: } (V_m/V_1) = (V_0/V_1)^{1 - n_m} \quad \text{(Eq. 7)}$$

where $n_m = 0.49$ (the H_2O/D_2O ratio at the midpoint), V_m/V_1 equals the midpoint partial solvent isotope effect, and V_0/V_1 represents the total isotope effect ((velocity in 100% H_2O)/(velocity in 100% D_2O)). The experimental and calculated midpoint partial isotope effects are presented in Table 2. The presence of D_2O lowered the catalytic activity of *Pt*NHase, resulting in a solvent isotope effect of 2.07 (Fig. 3). The plot of the atom fraction of deuterium *versus* V_n/V_1 ((velocity at *n* fraction of deuterium)/(velocity in 100% D_2O)) obtained for the reaction of benzonitrile and *Pt*NHase was best fit to Equation 6, suggesting that two protons are transferred during the rate-limiting step at pH 7.6. However, midpoint partial isotope effect calculations do not strongly distinguish between two protons transferred and generalized solvent effects (Table 2). Because the K_m was found to be independent of pH over the entire pH range studied, the $^D(k_{cat}/K_m)$ for *Pt*NHase is 1.7.

Temperature Dependence of K_m and k_{cat} for PtNHase—It was reported previously that *Pt*NHase is stable at 60 °C and pH 7.6 (35). These data are very unusual because most enzymes undergo some denaturation at temperatures above 50 °C, resulting in a decrease in V_{max} (28). This observed thermal stability provides the unique opportunity to probe the thermodynamic properties of the *Pt*NHase-catalyzed hydration of benzonitrile. Initially, the hydration rate of benzonitrile was measured in triplicate between 20 and 60 °C for *Pt*NHase at eight substrate concentrations ranging from 2 to 100 μM. From these data, both K_m and k_{cat} values were derived by fitting the experimental data to the Michaelis-Menten equation at each temperature studied. Both the k_{cat} and K_m values increased with increasing temperature.

In a simple rapid equilibrium, $V_{max}/[E] = k_{cat}$, the first-order rate constant. Keeping a constant enzyme concentration, an Arrhenius plot was constructed by plotting $\ln(k_{cat})$ *versus* $1/T$. A linear plot was obtained, indicating that the rate-limiting step does not change as the temperature is increased (28). From the slope of the line, the activation energy (E_a) for temperatures between 293 and 333 K was calculated to be 23.0 ± 1.2 kJ/mol (36). Because the slope of an Arrhenius plot is equal to $-E_{a1}/R$ (where $R = 8.3145\ J\cdot K^{-1}\cdot mol^{-1}$), other thermodynamic parameters were calculated by the following relations: $\Delta G^{\ddagger} = -RT\ln(k_{cat}h/k_BT)$, $\Delta H^{\ddagger} = E_a - RT$, and $\Delta S^{\ddagger} = (\Delta H^{\ddagger} - \Delta G^{\ddagger})/T$, where k_B, h, and R are the Boltzmann, Planck, and gas constants, respectively (Table 3). Assuming that the K_d is equal to the K_m, a linear plot was obtained for $\ln(1/K_m)$ *versus* $1/T$, which provides ΔH^0 by multiplying the negative slope by R. The following thermodynamic parameters were calculated by the relations: $\Delta G^0 = -RT\ln(1/K_m)$ and $\Delta S^0 = (\Delta H^0 - \Delta G^0)/T$ (Table 3).

Given the thermal stability of *Pt*NHase, the pH dependence of k_{cat} at saturating substrate concentrations (100 μM) at several pH values between 3.2 and 10.5 were also examined at three different temperatures to determine the identity of the ionizing groups exhibiting the pK_{ES1} and pK_{ES2} values of 5.9 and 9.2, respectively. These data were fit to Equation 1, providing three ionization constants, one for each temperature. A plot of ionization constants *versus* inverse absolute temperature yields the slope (Equation 8),

$$\text{Slope} = \Delta H_{ion}/2.303 \cdot R \quad \text{(Eq. 8)}$$

where R is the gas constant (Fig. 4, *A* and *B*) (37). The enthalpies of ionization calculated from these data are 7.6 ± 0.3 and 12.0 ± 0.3 kcal/mol, respectively. The enthalpy of ionization for pK_{ES1} is in the range for tyrosine or histidine residues (6.0–7.5 kcal/mol), suggesting that the pK_{ES1} is due to βTyr^{68} because no active-site histidine residues exist (34, 38). The enthalpy of ionization for pK_{ES2} is in the range for serine or arginine residues (12–13 kcal/mol), so it can be assigned to one of the following residues: αArg^{52}, αArg^{157}, or αSer^{112} (34, 38).

DISCUSSION

Simple catalytic mechanisms for NHases have been proposed based on x-ray crystal structures, theoretical modeling studies, synthetic models, and limited kinetic and spectroscopic studies (5, 16, 26, 39). In the most widely accepted mechanism of NHases, the nitrile moiety of the substrate binds directly to the metal center, displacing the active-site water/hydroxide group and allowing the metal ion to act as a Lewis acid, activating the coordinated nitrile toward nucleophilic attack (26). In this mechanism, the nucleophilic water/hydroxide is likely provided/activated by an active-site base. This mechanism was proposed based on observed changes in electronic absorption and EPR spectra upon the addition of nitriles (39). In addition, synthetic model studies have revealed that nitriles can readily exchange with low spin Fe(III) and Co(III) centers (40, 41).

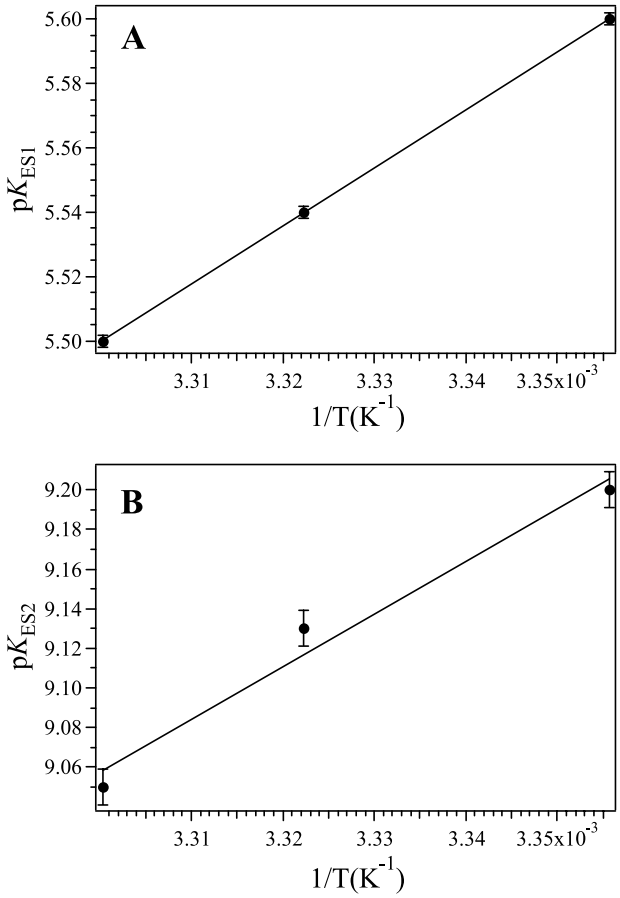

FIGURE 4. **Plots of the ionization constants pK_{ES1} (*A*) and pK_{ES2} (*B*) *versus* 1/*T* for the hydration of benzonitrile catalyzed by *Pt*NHase.**

Recently, the x-ray crystal structure of the NO-bound iron-type NHase from *Rhodococcus erythropolis* revealed that NO binds in place of the metal-coordinated water molecule in the wild-type enzyme (42). In addition, the x-ray crystal structure of the cobalt-type NHase from *P. thermophila* bound by the weak competitive inhibitor *n*-butyric acid revealed that a carboxylate oxygen atom binds to the metal ion, displacing the metal-coordinated water molecule (20). Both of these structural studies are consistent with the direct interaction of the nitrile with the active-site metal ion. Moreover, theoretical modeling studies have suggested that nitriles can be accommodated in the active site of the NHase from *R. erythropolis* and that the nitrile can bind to the active-site metal (26, 43). However, to date, no detailed catalytic mechanism has been proposed for any NHase, in part because of a lack of detailed kinetic studies.

To examine the reaction mechanism of *Pt*NHase, we initially examined the kinetic parameters k_{cat}, K_m, and k_{cat}/K_m for the hydration of benzonitrile as a function of pH. *Pt*NHase was found to exhibit a bell-shaped curve for plots of relative activity *versus* pH at pH 3.2–11. These data compare well with a plot of activity *versus* pH reported for the cobalt-type NHase from *Pseudomonas putida* NRRL 18668 (44). Inspection of a plot of $\log(K_m)$ *versus* pH indicated that the K_m does not vary with pH. These data suggest that the substrate does not get ionized. Therefore, plots of $\log(k_{cat})$ *versus* pH and plots of $\log(k_{cat}/K_m)$ *versus* pH provide similar pK_a values.

Examination of a plot of $\log(k_{cat})$ *versus* pH revealed a bell-shaped curve that yielded a pK_{ES1} value of 5.9 ± 0.1 and a pK_{ES2} value of 9.2 ± 0.1 ($k_{cat}' = 130 \pm 1.0\ s^{-1}$). The slopes of the asymptotes, calculated as described previously (30), of the acidic and basic limbs of $\log(k_{cat})$ *versus* pH for *Pt*NHase are 1, indicating that one group is ionized on each limb. These data indicate that one ionizable group (pK_{ES1}) must be deprotonated and that a second ionizable group must be in the protonated form (pK_{ES2}) in the *E*S complex for catalysis to occur. Assignment of the observed pK_{ES} values is difficult, but likely candidates for pK_{ES1} are the deprotonation of the metal-coordinated sulfinic acid (putative pK_a in NHase of 7.6) (24) and the protonation of the leaving group or an active-site residue such as βTyr^{68}. Based on the temperature dependence of the ionization constant, the most likely assignment for pK_{ES1} is βTyr^{68}. The observed pK_{ES1} value cannot be the metal-bound water molecule because ENDOR data recorded in both ^1H_2O and ^2H_2O as well as in ^{17}O-labeled water on the iron-type NHase from *Brevibacterium* sp. strain R312 indicate that a water molecule is bound to the metal center at pH 7.5 (45). The observed pK_{ES2} value may be due to the deprotonation of a conserved active-site arginine residue (βArg^{52} or βArg^{157}) that forms a hydrogen bond with both the sulfenic and sulfinic acid ligands of the active site (20). Alternatively, the pK_{ES2} value may be due to the deprotonation of αSer^{112} or the metal-bound water molecule depending on which proposed mechanism is active. Based on the temperature dependence of the ionization constant, the second ionization constant pK_{ES2} is best assigned to either an active-site arginine residue or αSer^{112}.

Enzyme-centered ionizable groups were gleaned from plots of $\log(k_{cat}/K_m)$ *versus* pH because it is possible to determine p*K* values centered on the free enzyme and free substrate (46). Similar to the plots of $\log(k_{cat})$ *versus* pH, fits of $\log(k_{cat}/K_m)$ *versus* pH provided a pK_{E1} value of 5.8 ± 0.1 and a pK_{E2} value of 9.1 ± 0.1 ($k_{cat}'/K_m' = (6.5 \pm 0.1) \times 10^3\ s^{-1}\ mM^{-1}$). Both asymptotes have slopes of ~1, indicating that a single ionizable group exists at both high and low pH values. Similar to pK_{ES1}, the pK_{E1} value is most likely due to βTyr^{68}, but could also be due to the deprotonation of the metal-coordinated sulfinic acid. Moreover, similar to pK_{ES2}, the enzyme-centered pK_{E2} value is most likely due to αSer^{112}, but may also be due to βArg^{52} or βArg^{157}, all of which are strictly conserved.

A very fundamental aspect of the catalytic mechanism of NHases that has not been addressed to date is the chemical identity of the rate-limiting step. Kinetic isotope effect studies are an excellent way to gain an understanding of the nature of the rate-limiting step as well as to probe the transition state of catalytic reactions (47). Primary isotope effects are observed if a bond to the labeled atom is made or broken during the reaction, whereas secondary isotope effects describe processes at other positions. Therefore, we examined the solvent isotope effect of *Pt*NHase using benzonitrile as the substrate at pH 7.6 (p^2H = p^1H meter reading + 0.4) (27) by substituting hydrogen (^1H) with deuterium (^2H). The intrinsic primary isotope effect (k_H/k_D) is related to the symmetry of the transition state for that step (*i.e.* the larger the isotope effect, the more symmetrical the transition state), with the theoretical limit being 9 at 37 °C in the absence of tunneling effects. For the simplest case, in which

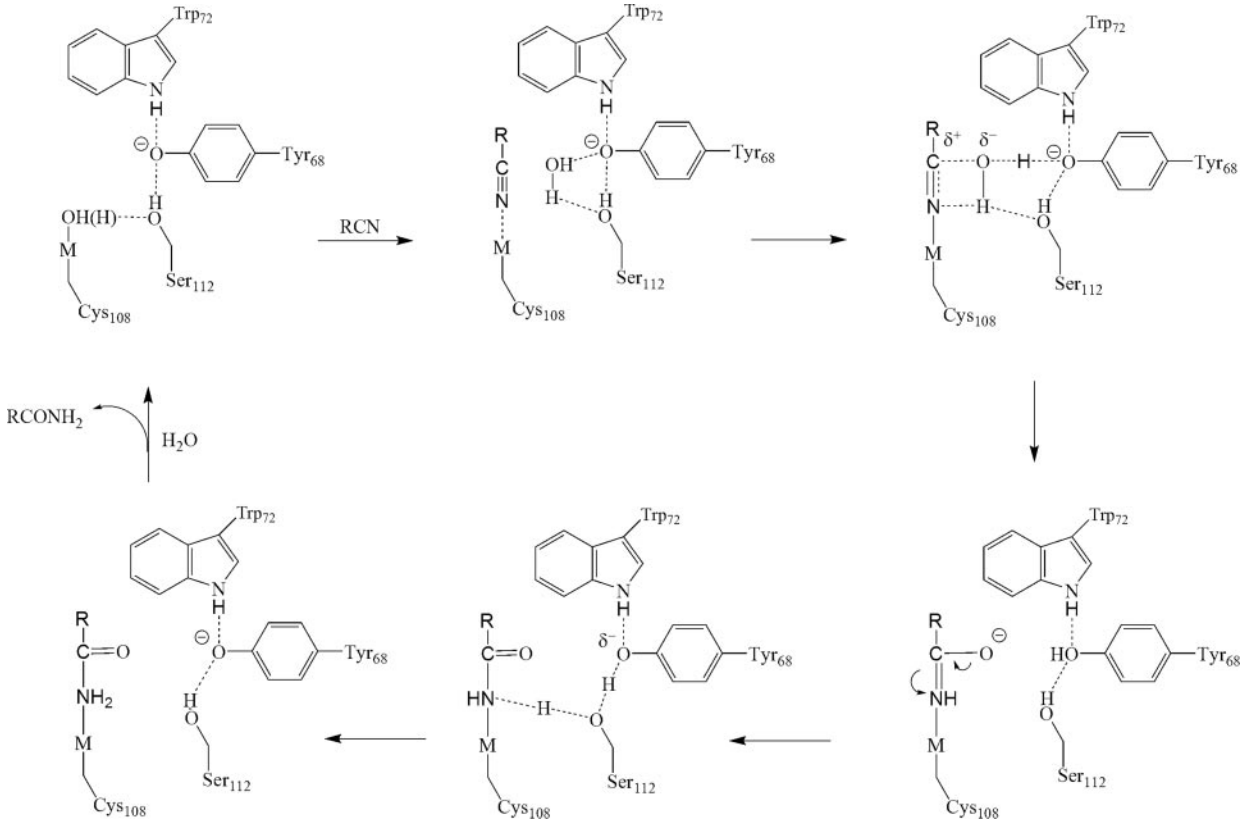

FIGURE 5. **Proposed catalytic mechanism for NHases.**

a single proton produces the solvent isotope effect, a plot of the atom fraction of deuterium *versus* V_n/V_D would be linear, where V_n is the k_{cat} at a particular fraction of deuterium and V_D is the k_{cat} in buffer containing 100% deuterium oxide (33). The presence of D_2O lowers the catalytic activity of *Pt*NHase, resulting in a solvent isotope effect of 2.07. This normal isotope effect suggests that an oxygen–hydrogen bond is broken in the rate-limiting step. For *Pt*NHase, V_n/V_0 deviates from linearity, and the best fit indicates that two protons are transferred during catalysis with similar fractionation factors (0.66 and 0.68). Analysis of the midpoint solvent isotope effect also supports involvement of two protons in the reaction. These data may reflect the transfer of a proton from an active-site water molecule to an active-site base to form a more nucleophilic hydroxide and the transfer of a proton from the hydroxyl group of the imine intermediate to form the amide. Conversely, they may represent the transfer of a proton from the hydroxyl group of the imine intermediate to an active-site base, followed by the transfer of a proton from a base to the imine to form the amide. The first fractionation factor ($\phi_{T1} = 0.66$) is characteristic of a proton–oxygen bond (neutral oxygen, 0.8–1.2) with a conventional isotope effect equal to 1 (32). It is likely that, at pH 7.6, the protonation state of βTyr^{68} (pK_a in the enzyme-substrate complex of 5.9 ± 0.1) results in the transfer of a proton to αSer^{112}, which eventually donates that proton to the leaving group.

The rate-limiting step in the catalytic reaction is important in understanding the hydration of benzonitrile by *Pt*NHase. Because *Pt*NHase is stable at 60 °C, *Pt*NHase provides the unique opportunity to determine the activation parameters of the *ES*‡ complex over a wide temperature range. Construction of an Arrhenius plot for the hydration of benzonitrile by *Pt*NHase indicated that the rate-limiting step does not change as a function of temperature (38). The E_a for the activated *ES*‡ complex is 23.0 ± 0.12 kJ/mol for *Pt*NHase, which is 60% of the value reported for the iron-type NHase from *Brevibacterium imperialis* CBS 489-74 (38.4 kJ/mol), suggesting that transition state formation is more viable for the Co(III) enzyme (48). The enthalpy of activation calculated over the temperature range 20–60 °C is 18.0 ± 0.9 kJ/mol, whereas that for *Pt*NHase at 25 °C is −146.0 ± 0.7 J/mol. The positive enthalpy is indicative of a conformation change upon substrate binding, likely due to the energy of bond formation and breaking during nucleophilic attack on the scissile carbon–nitrogen triple bond of the substrate. On the other hand, the negative entropy suggests that some of the molecular motions are lost upon *ES*‡ complex formation, possibly due to hydrogen bond formation between catalytically important amino acids, water molecules, and the substrate. This is consistent with the proton inventory data obtained at pH 7.6, where multiple proton exchanges take place. All of these factors contribute to the positive free energy of activation. Because the K_m also increases with temperature, the thermodynamic parameters for the formation of the Michaelis complex at 25 °C were also determined. The observed negative ΔG^0 value indicates that the formation of the *ES* complex is thermodynamically favorable and that the reaction catalyzed by *Pt*NHase is slightly exothermic. However, ΔS^0 was found to be negative, suggesting the *ES* complex is highly

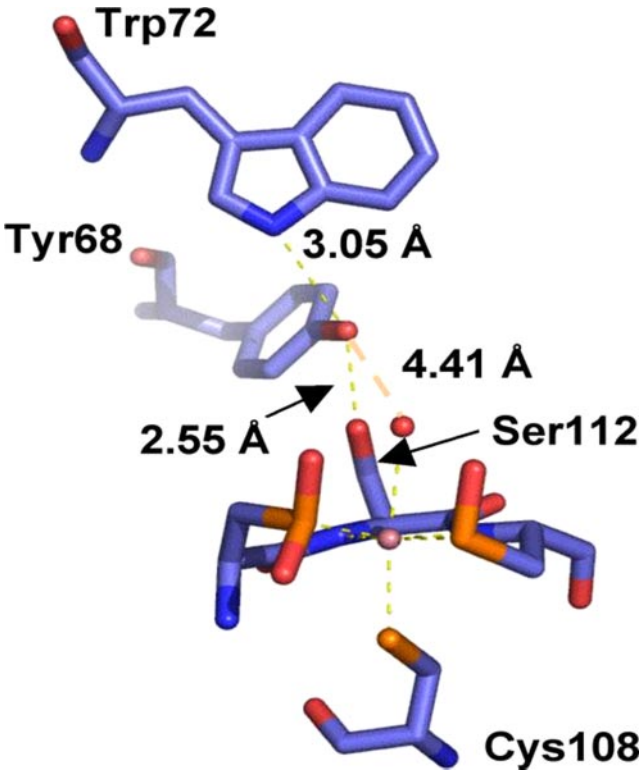

FIGURE 6. **Active sites of the NHases from *P. thermophila*, including the active-site triad (Protein Data Bank code 1IRE) (20, 21).**

ordered, possibly due to an extensive hydrogen bond network consistent with the observed solvent isotope effect.

Based on the data presented herein and the previously reported x-ray crystal structures and kinetic, spectroscopic, theoretical modeling, and synthetic model complex studies (5, 16, 26, 39), a detailed catalytic mechanism for NHases can be proposed (Fig. 5). This mechanism is based on the proposal that nitriles bind directly to the trivalent metal ion active site, which is supported by kinetic, EPR, UV-visible, and theoretical modeling studies (5, 16, 26, 39). Therefore, we propose that the nitrile nitrogen atom coordinates to the active-site metal ion, displacing the metal-bound water molecule. Once nitrile binding occurs, both an active-site water molecule and an active-site base are needed for the reaction to proceed (5, 16, 26, 39). Based on sequence alignment of the β-subunits of the crystallographically characterized cobalt- and iron-type NHases and several non-crystallographically characterized NHases, we recognized that the motif YYE(H/K)(W/Y) (residues 68–72 in *Pt*NHase numbering) is strictly conserved. Interestingly, the strictly conserved residue αSer^{112} appears to form a catalytic triad with βTyr^{68} and βTrp^{72} in *Pt*NHase (Fig. 6). This catalytic triad is reminiscent of those observed in non-metallodehydrogenases (49). For example, 2-[(*R*)-2-hydroxypropylthio]ethanesulfonate dehydrogenase utilizes a Lys-Tyr-Ser triad, and the tyrosine residue is deprotonated at pH 7.5 (pK_a of 6.9) (50, 51). Given that a nearly identical catalytic triad exists in all NHases, we propose that one or more of the residues of this catalytic triad function as general bases. We propose that, like 2-[(*R*)-2-hydroxypropylthio]ethanesulfonate dehydrogenase, βTyr^{68} in *Pt*NHase is deprotonated at pH 7.6 and that this deprotonation process is likely the observed pK_a value of 5.9. That βTyr^{68} plays an important catalytic role is consistent with the observed 17-fold decrease in k_{cat} when βTyr^{68} is substituted with Phe (20). The fact that K_m also increases by >10-fold upon substitution of βTyr^{68} with Phe indicates that βTyr^{68} also functions to bind and position substrate, likely stabilizing the transition state. Because the observed 17-fold decrease in k_{cat} when βTyr^{68} is substituted with Phe is not that expected for a general base, the strictly conserved residue αSer^{112}, which is also part of the proposed catalytic triad, likely functions as the general base by deprotonating βTyr^{68}. Displacement of the metal-bound water molecule by a nitrile will activate the carbon–nitrogen bond toward nucleophilic attack and likely place the water molecule in the proper orientation, with regard to the catalytic triad and the carbon–nitrogen bond, for the addition of an oxygen–hydrogen bond across the carbon–nitrogen bond. Based on our preliminary isotope studies, two protons are transferred in the transition state, which we propose is due to a water proton being transferred to the nitrile nitrogen atom and the second to βTry^{68}, consistent with our observed normal isotope effect. Once proton transfer occurs, the resulting imidate can tautomerize to form an amide with a subsequent proton transfer from αSer^{112}, which functions to shuttle protons from βTyr^{68}. Finally, the amide product can be displaced by a water molecule, providing the regenerated catalyst.

Acknowledgment—We thank Dr. Alvan C. Hengge for helpful discussions.

REFERENCES

1. Petrillo, K. L., Wu, S., Hann, E. C., Cooling, F. B., Ben-Bassat, A., Gavagan, J. E., Dicosimo, R., and Payne, M. S. (2005) *Appl. Microbiol. Biotechnol.* **67,** 664–670
2. Padmakumar, R., and Oriel, P. (1999) *Appl. Biochem. Biotechnol.* **77–79,** 671–679
3. Nagasawa, T., and Yamada, H. (1995) *Pure Appl. Chem.* **67,** 1241–1256
4. Mylerova, V., and Martinkova, L. (2003) *Curr. Org. Chem.* **7,** 1–17
5. Kovacs, J. A. (2004) *Chem. Rev.* **104,** 825–848
6. Banerjee, A., Sharma, R., and Banerjee, U. C. (2002) *Appl. Microbiol. Biotechnol.* **60,** 33–44
7. Kobayashi, M., Nagasawa, T., and Yamada, H. (1992) *Trends Biotechnol.* **10,** 402–408
8. Nagasawa, T., Shimizu, H., and Yamada, H. (1993) *Appl. Microbiol. Biotechnol.* **40,** 189–195
9. Yamada, H., and Kobayashi, M. (1996) *Biosci. Biotechnol. Biochem.* **60,** 1391–1400
10. Nagasawa, T., Mathew, C. D., Mauger, J., and Yamada, H. (1988) *Appl. Environ. Microbiol.* **54,** 1766–1770
11. Shaw, N. M., Robins, K. T., and Kiener, A. (2003) *Adv. Synth. Catal.* **345,** 425–435
12. Wu, Z. L., and Li, Z. Y. (2003) *Chem. Commun.* (*Camb.*) **3,** 386–387
13. Dadd, M. R., Claridge, T. D., Walton, R., Pettman, A. J., and Knowles, C. J. (2001) *Enzyme Microb. Technol.* **29,** 20–27
14. Martnkov, L., Klempier, N., Prepechalov, I., Prikrylov, V., Ovesn, M., Griengl, H., and Kren, V. (1998) *Biotechnol. Lett.* **20,** 909–912
15. Endo, I., Nojiri, M., Tsujimura, M., Nakasako, M., Nagashima, S., Yohda, M., and Odaka, M. (2001) *J. Inorg. Biochem.* **83,** 247–253
16. Harrop, T. C., and Mascharak, P. K. (2004) *Acc. Chem. Res.* **37,** 253–260
17. Hourai, S., Miki, M., Takashima, Y., Mitsuda, S., and Yanagi, K. (2003) *Biochem. Biophys. Res. Commun.* **312,** 340–345
18. Huang, W., Jia, J., Cummings, J., Nelson, M., Schneider, G., and Lindqvist, Y. (1997) *Structure* **5,** 691–699

19. Miyanaga, A., Fushinobu, S., Ito, K., and Wakagi, T. (2001) *Biochem. Biophys. Res. Commun.* **288,** 1169–1174
20. Miyanaga, A., Fushinobu, S., Ito, K., Shoun, H., and Wakagi, T. (2004) *Eur. J. Biochem.* **271,** 429–438
21. Deleted in proof
22. Nakasako, M., Odaka, M., Yohda, M., Dohmae, N., Takio, K., Kamiya, N., and Endo, I. (1999) *Biochemistry* **38,** 9887–9898
23. Tsujimura, M., Odaka, M., Nakayama, H., Dohmae, N., Koshino, H., Asami, T., Hoshino, M., Takio, K., Yoshida, S., Maeda, M., and Endo, I. (2003) *J. Am. Chem. Soc.* **125,** 11532–11538
24. Dey, A., Chow, M., Taniguchi, K., Lugo-Mas, P., Davin, S., Maeda, M., Kovacs, J. A., Odaka, M., Hodgson, K. O., Hedman, B., and Solomon, E. I. (2006) *J. Am. Chem. Soc.* **128,** 533–541
25. Boone, A. J., Cory, M. G., Scott, M. J., Zerner, M. C., and Richards, N. G. (2001) *Inorg. Chem.* **40,** 1837–1845
26. Desai, L. V., and Zimmer, M. (2004) *Dalton Trans.* **6,** 872–877
27. Salomaa, P., Schaleger, L. L., and Long, F. A. (1964) *J. Am. Chem. Soc.* **86,** 1–7
28. Segel, I. H. (1975) *Enzyme Kinetics: Behavior and Analysis of Rapid Equilibrium and Steady-State Enzyme Systems*, John Wiley & Sons, Inc., New York
29. Cornish-Bowden, A. (1995) *Fundamentals of Enzyme Kinetics*, 2nd Ed., Portland Press, London
30. Cleland, W. W. (1997) *Adv. Enzymol. Relat. Areas Mol. Biol.* **45,** 273–387
31. Albery, W. J. (1975) *Proton Transfer Reactions*, Chapman & Hall, London
32. Venkatasubban, K. S., and Schowen, R. L. (1984) *CRC Crit. Rev. Biochem.* **17,** 1–44
33. Elrod, J. P., Hogg, J. L., Quinn, D. M., Venkatasubban, K. S., and Schowen, R. L. (1980) *J. Am. Chem. Soc.* **102,** 3917–3922
34. Izatt, R. M., and Christensen, J. J. (1976) *Heats of Proton Ionization, pK, and Related Thermodynamic Quantities*, 3rd Ed., CRC Press, Cleveland, OH
35. Yamaki, T., Oikawa, T., Ito, K., and Nakamura, T. (1997) *J. Ferment. Bioeng.* **83,** 474–477
36. Chen, G., Edwards, T., D'Souza, V. M., and Holz, R. C. (1997) *Biochemistry* **36,** 4278–4286
37. Bienvenue, D. L., Mathew, R. S., Ringe, D., and Holz, R. C. (2002) *J. Biol. Inorg. Chem.* **7,** 129–135
38. Segel, I. H. (1993) *Enzyme Kinetics: Behavior and Analysis of Rapid Equilibrium and Steady-State Enzyme Systems*, Wiley Classics Library Ed., John Wiley & Sons, Inc., New York
39. Sugiura, Y., Kuwahara, J., Nagasawa, T., and Yamada, H. (1987) *J. Am. Chem. Soc.* **109,** 5848–5850
40. Shearer, J., Jackson, H. L., Schweitzer, D., Rittenberg, D. K., Leavy, T. M., Kaminsky, W., Scarrow, R. C., and Kovacs, J. A. (2002) *J. Am. Chem. Soc.* **124,** 11417–11428
41. Shearer, J., Kung, I. Y., Lovell, S., Kaminsky, W., and Kovacs, J. A. (2001) *J. Am. Chem. Soc.* **123,** 463–468
42. Nagashima, S., Nakasako, M., Dohmae, N., Tsujimura, M., Takio, K., Odaka, M., Yohda, M., Kamiya, N., and Endo, I. (1998) *Nat. Struct. Biol.* **5,** 347–351
43. Greene, S. N., and Richards, N. G. J. (2006) *Inorg. Chem.* **45,** 17–36
44. Payne, M. S., Wu, S., Fallon, R. D., Tudor, G., Stieglitz, B., Turner, I. M., and Nelson, M. J. (1997) *Biochemistry* **36,** 5447–5454
45. Jin, H., Turner, I. M., Nelson, M. J., Gurbiel, R. J., Doan, P. E., and Hoffman, B. M. (1993) *J. Am. Chem. Soc.* **115,** 5290–5291
46. Dixon, M., and Webb, E. C. (1979) *Enzymes*, 3rd Ed., Academic Press, New York
47. Cleland, W. W. (1982) *CRC Crit. Rev. Biochem.* **13,** 385–427
48. Alfani, F., Cantarella, M., Spera, A., and Viparelli, P. (2001) *J. Mol. Catal. B* **11,** 687–697
49. Jones, S., and Thornton, J. M. (2004) *Curr. Opin. Chem. Biol.* **8,** 3–7
50. Clark, D. D., Boyd, J. M., and Ensign, S. A. (2004) *Biochemistry* **43,** 6763–6771
51. Clark, D. D., and Ensign, S. A. (2002) *Biochemistry* **41,** 2727–2740

Unraveling the Catalytic Mechanism of Nitrile Hydratases

Sanghamitra Mitra and Richard C. Holz

J. Biol. Chem. 2007, 282:7397-7404.
doi: 10.1074/jbc.M604117200 originally published online December 6, 2006
